# A NOVEL METHOD FOR OPTICALLY MONITORING PV TRACKING SYSTEMS INCLINATION USING WAVELET TRANSFORMS AND NEURAL NETWORKS

**Ali M. J. Al-Lawati**
Dept. of Electrical and Computer Engineering, College of Engineering, Sultan Qaboos University
P.O. Box 33, Al Khoud, PC 123, Sultanate of Oman, Tel.(+968)24141328, Fax(+968)24413454

***Abstract:*** *This work demonstrates the feasibility of utilizing optical images of PV modules or arrays controlled by tracking systems to determine its tilt angle. The proposed novel method uses discrete wavelet transforms and artificial neural networks. The process can be accomplished remotely to reduce the need of manpower and time required to find the tracking systems inclination angle. Hardware and software needed is relatively simple. Application of this method can be extended to other systems such as solar thermal collectors. Proposed algorithms performance, using different artificial neural network parameters and families of wavelet transforms, is also investigated. All combinations illustrate the reliability and practicality of the proposed method. Moreover, in order to account for noisy images, the performance is examined under different values of signal to noise ratios, the method performed very well at all noise levels introduced.*

***Key words:*** *PV tracking; DWT; ANN.*

***Abbreviations and symbols***

| | |
|---|---|
| PV | Photo Voltaic |
| DWT | Discrete Wavelet Transform |
| 2-D DWT | Two dimensional Discrete Wavelet Transform |
| ANN | Artificial Neural networks |
| *i*, | input fed to ANN |
| *w* | ANN weights matrix |
| *b* | ANN bias vector |
| *f* | activation function |
| o | ANN output vector |
| *n* | discrete functions index |
| *M* | number of pints in a discrete signal *J* dilation or scaling coefficient |
| *K* | position or translation coefficient |
| $\psi$ | wavelet function |
| $\phi$ | dilation function. |
| *Dh* | horizontal details coefficients in 2-D DWT |
| *Dv* | vertical details coefficients in 2-D DWT |
| *Dd* | diagonal details coefficients in 2-D DWT |
| *A* | approximation coefficients in 2-D DWT |
| *db* | Daubechies wavelet |
| *coif* | Coiflets wavelet |
| *sym* | Symlets wavelet |
| SNR | Signal to Noise Ratios |
| MAE | Mean Absolute Error |

## *1. Introduction*

The growing use of renewable energy resources across the globe has improved the performance of renewable energy systems. Applications utilizing solar energy in particular, are increasingly deployed in many regions of the world [1]. One of its main drivers is the possibility of direct conversion of solar radiation into electricity using photo voltaic (PV) modules and arrays [2]. PV systems produce electrical energy by collecting solar radiation, thus are usually desired to be perpendicular to the sun [3]. This can be achieved by deploying solar tracking systems. Tracking systems can improve generated power by up to 30% to 40% , depending on the number of tracking axis used [4] and [5].

Solar energy plants can host hundreds of PV modules, arrays and solar thermal collectors. The alignment and positioning of solar tracking systems should be regularly inspected to assure its proper and optimal functioning [6]. Inspecting tracking systems having a large number of elements requires verifying the arrays or modules tilt angles individually. This in turn requires dedicated manpower and time. The process can be automated using traditional sensors that feedback the tilt angles or positions to a central location. The size and cost of such sensors network could be significant.

This work introduces a novel and cost effective method to determine the inclination or tilt angle of a solar tracking system by examining each module or

array individually using optical images of the solar energy plant. Although the described application is PV oriented, the proposed method can be applied to solar thermal collectors and other applications.

The requirements of such a system are minimal, namely: a camera and a PC which can run the software implementing the proposed algorithms. Moreover, the proposed method allows remote monitoring of the tracking system, which is usually located at remote locations. This is possible if images are available. Images could be acquired by ordinary acquisition devices such as a web cam or satellite based optical imaging systems.

### *2.Theory*

The present work utilizes the strength of both, the Discrete Wavelet Transform (DWT) and Artificial Neural networks (ANN) as discussed in the following sections.

### *2.1 Artificial Neural Networks*

ANNs are algorithms that can learn in a self organizing way that emulates biological neural networks. ANNs can deal with noisy, inconsistent and fuzzy data [7].

ANNs are described mainly by their architectures, training algorithms and activation functions as shown in figure 1. The architecture illustrates a typical layer of neurons. Three neurons are shown in this example, the same number of neurons used in the implementation of this work. The interconnections layer is also know as the hidden layer. In addition to the hidden layer, the network consists of an input and an output layer. The training algorithms determine weights or significance of information passing through each of these interconnections. These weights could be fixed values or could be based on a series of updated data. ANNs with the later type of weights is known as an unsupervised network. The weights can be determined by training the network using series of input and output data. The present work depends on this category of ANNs known as supervised networks. Activation functions explain the dependence of a neurons output on its input. Activation functions can also be associated with weights known as biases. In general, for an input vector *i*, fed to an ANN with weights matrix *w* and bias vector *b* where *w* and *b* are determined by a certain training algorithm, and an activation function *f*; the output vector, *o*, of such a system is given by:

$$o = f(wi + b) \quad (1)$$

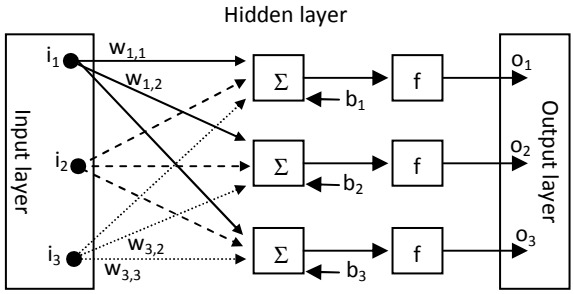


**Figure1**. ANN architecture with 3 neurons in the hidden layer

A common application of ANNs is recognition of certain shapes or patterns it was taught in advance to identify [8]. The network is trained using a set of input and output data prior to the application. Performance of such networks can be evaluated by introducing inputs of known outputs known as validation data. Differences between outputs predicted by the ANN and validation data can be then used to evaluate the network performance [9].

### *2.2. Wavelet Transforms*

Wavelet transforms were discovered by a French engineer, Jean Morlet, in 1982 [10]. It offers the possibility of reliable parameter estimation when used as a multi-resolution analysis technique [11]. Wavelet transforms can also be considered as an extension to the Fourier transform which is limited to only time and frequency scales. In this work, DWT was used and will be explained below. For information on continues wavelet transforms and its relation to DWT and Fourier transform refer to [10] and [12].

Applying DWT to a signal implies applying band pass filtering several times. The signal is decomposed into a low pass component known as approximations and a high pass component known as details [13]. The filtering is followed by down sampling. Subsequent stages repeat, this two component filtering, on the approximations at each level. Figure 2 illustrates the DWT implementation process.

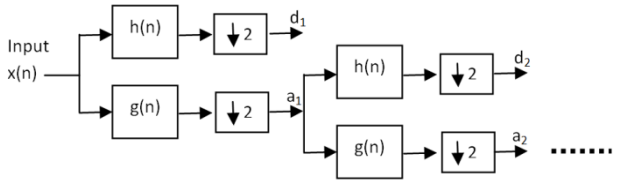


**Figure2**. DWT process for discrete signal x(n), h(n) and g(n) are high pass and low pass filters respectively, d: details and a: approximations.

The wavelet transform can be mathematically be expressed as [14]:

$$x[n] = \frac{1}{\sqrt{M}}\sum_k W_\emptyset[j_0,k]\emptyset_{j_0,k}[n] + \frac{1}{\sqrt{M}}\sum_{j=j_0}^{\infty}\sum_k W_\psi[j,k]\,\psi_{j,k}[n] \quad (2)$$

Where all functions containing variable [$n$] are discrete functions defined in [0, $M$-1], for a total of $M$ points, $j$: dilation or scaling coefficient, $k$: position or translation coefficient, $W$: wavelet coefficients span, $\psi$: wavelet function and $\phi$: dilation function.

The approximations and details can also be found using the following two equations respectively:

$$W_\emptyset[j_0,k] = \frac{1}{\sqrt{M}}\sum_n x[n]\emptyset_{j_0,k}[n] \quad (3)$$

$$W_\psi[j_0,k] = \frac{1}{\sqrt{M}}\sum_n x[n]\,\psi_{j,k}[n] \;\; j \geq j_0 \quad (4)$$

Since images are 2-D data representations, assuming a single color processing, a 2D-DWT is required to process images. The filtering possibilities are not just high pass (*H*) or low pass (*L*) as shown in figure 2, it could be (*L*) then (*L*), (*L*) then (*H*), (*H*) then (*L*) or (*H*) then (*H*) again. Therefore, in 2D decompositions, images are transformed into four sub sets. The subsets are the approximation coefficients, which represent a lower resolution of the original image, and three details coefficients representing horizontal, vertical and diagonal coefficients of the image.

### *3. Material and Methods*

Images of PV modules at different tilt angles were used to determine the modules inclination angles. Due to ANN's forgiving nature, the camera can be placed at many possible points as long as it can provide decent images. The ANN should still be able to determine the inclination, if it was trained on images acquired from the same shooting angle.

Processing large images is a burden from computational and time requirement points of view. Therefore, the main objective of this work is to demonstrate the possibility of using a reasonably small ANN that has few neurons but can still perform the required task of determining PV modules tilt angles. Moreover, In order to minimize the size of the data to be processed, yet retain the main features of the image, wavelet transforms were implemented prior to the ANN stage. Features extracted by the DWT, namely, the approximations and details of the PV images, were used to train the ANN.

#### *3.1 Image processing and DWT implementation*

Images were processed in the following order (summarized by figure 3):

(i) Acquire the PV module images at known inclination angles.
(ii) Separate modules images from the surroundings and background.
(iii) Resize images to have 256*265 points. This unifies images sizes.
(iv) Convert images to gray scale with values normalized to fall in the range of 0 to 1 ignoring other colors and apply a threshold.
(v) Apply 2D DWT to images to reach a decomposition level having only 8*8 elements in each of the three details coefficients, (horizontal: *Dh*, vertical: *Dv* & diagonal: *Dd*) and the approximation coefficient (*A*) as illustrated in figure 3. Several trials were performed to select the minimum usable coefficients size.

Commonly used wavelet transforms that are available in Matlab were selected to demonstrate the proposed method. In particular, Haar, Daubechies 4 (*db*4), Coiflets (*coif*1) and Symlets (*sym*3) wavelets were selected to carry out the implementation. Figures 4a, b, c and d are examples of such approximation and details images. In order to have an 8*8 size details and coefficients; different decomposition levels were applied in Matlab to the different wavelet families above.

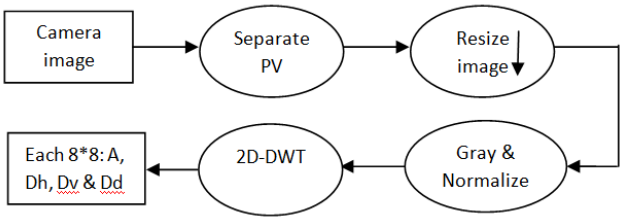


**Figure3**. Image processing and DWT stage

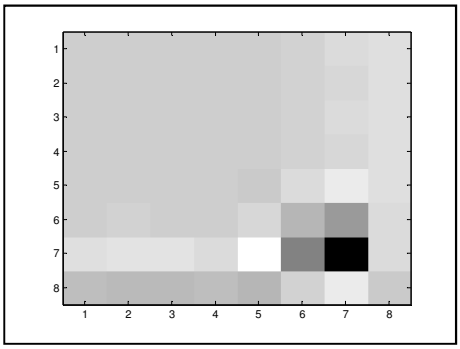

(a) Approximation coefficients

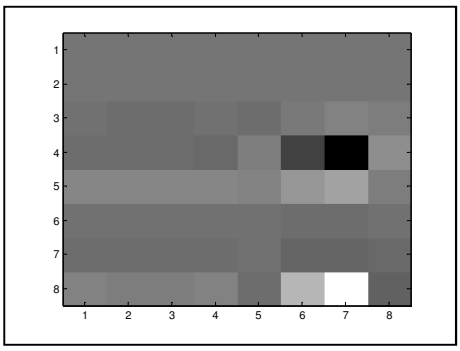

(b) Horizontal details coefficients

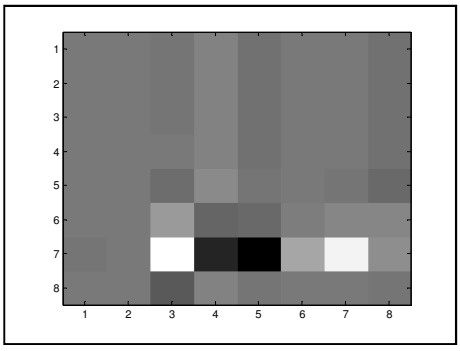

(c) Vertical details coefficients

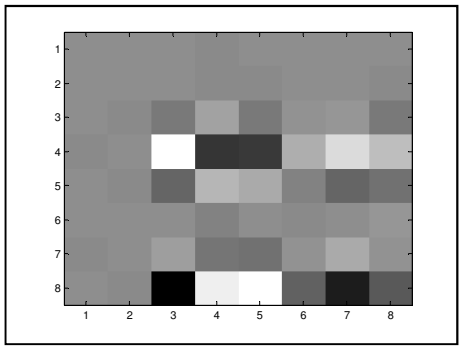

(d) Diagonal details coefficients

**Figure4**. Level 7, *db*4 coefficients for a PV module at an inclination angle of 60° and a SNR=3

### *3.2 ANN implementation*

A total of 5 sets of images were used. Each set consisted of 9 images representing a PV module tilted at angles 10°, 20°, … & 90°. 90° correspond to the case where the PV surface plane is perpendicular to a ray extending from the camera lens, which is far enough to be assumed as a point source, to the PV module. 0° on the other hand means the PV surface is parallel to the ray and cannot be seen by the camera.

In order to account for different image qualities and test the performance of the ANN at more challenging conditions, noise was introduced to 4 of the 5 sets (36 of the 45 images). The Signal to Noise Ratios (SNRs) of the sets were adjusted to be 3, 6, 9 and 12. Figure 5 illustrates a processed image of size 256*256 points at a SNR=12 and an inclination angle of 30°.

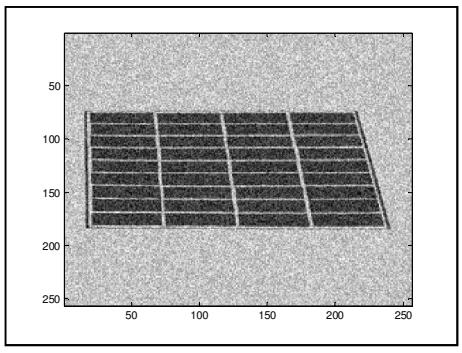

Figure5. A processed 256*256 image of a PV module at an inclination angle of 30° and a SNR=12.

A feed forward back propagation ANN was used (newff function in Matlab). In order to satisfy the requirement of a small number of neurons, only one

hidden layer with three neurons was used. Matlab transfer function (tansig), training function (trainlm) were used to construct and training the network.

Inputs to the ANN were *A*, *Dh*, *Dv* and *Dd*, whereas the output was the PV modules tilt or inclination angle. Fifteen combinations of the 45 images were used for training and validation trials. Each time, 7 tilt angles images were used for training and 2 angles images, not seen before by the ANN were used for validation. Every training and validation run for each set was repeated 100 times. The previous steps were repeated for 4 different values of training goals. This was repeated for Haar, *db*4, *coif*1 and *sym*3 wavelets.

### *4. Results and discussion of results*

Tables 1 to 4 illustrate the Mean Absolute Error (MAE) values using different wavelets. The error is the difference between the actual inclination angle, and the angle predicted by the ANN. Each set of the 15 sets corresponds to a certain combination of data used for training and validation. Each entry is based on data obtained from 100 runs of the algorithm. MAE for four different values of training goals are tabulated.

**Table1.** MAE values using Haar wavelet with different goal values and different training/validation images combinations.

| Goal | .0001 | .001 | .01 | .1 |
|---|---|---|---|---|
| Set# | | | | |
| 1 | 2.24 | 1.55 | 2.22 | 4.50 |
| 2 | 2.40 | 1.57 | 2.45 | 4.86 |
| 3 | 1.78 | 1.96 | 2.15 | 5.11 |
| 4 | 2.22 | 1.80 | 2.97 | 3.63 |
| 5 | 2.29 | 2.70 | 2.43 | 3.95 |
| 6 | 4.72 | 3.25 | 5.02 | 4.67 |
| 7 | 0.63 | 3.34 | 1.66 | 1.25 |
| 8 | 1.00 | 0.67 | 1.03 | 1.82 |
| 9 | 2.46 | 1.24 | 2.26 | 0.65 |
| 10 | 2.12 | 0.99 | 2.38 | 0.86 |
| 11 | 1.52 | 1.85 | 1.30 | 1.06 |
| 12 | 3.66 | 2.35 | 3.55 | 0.70 |
| 13 | 3.80 | 4.06 | 4.34 | 3.92 |
| 14 | 0.99 | 3.86 | 0.36 | 2.58 |
| 15 | 3.59 | 1.48 | 3.04 | 2.53 |

**Table2.** MAE values using *db*4 wavelet with different goal values and different training/validation images combinations.

| Goal | .0001 | .001 | .01 | .1 |
|---|---|---|---|---|
| Set# | | | | |
| 1 | 2.22 | 2.03 | 2.20 | 1.89 |
| 2 | 2.55 | 3.19 | 2.64 | 1.65 |
| 3 | 5.75 | 5.85 | 4.31 | 3.02 |
| 4 | 4.40 | 3.75 | 6.38 | 4.21 |
| 5 | 2.41 | 2.30 | 2.68 | 3.60 |
| 6 | 4.25 | 3.73 | 3.49 | 4.37 |
| 7 | 4.27 | 3.89 | 3.78 | 4.93 |
| 8 | 4.27 | 6.70 | 3.74 | 5.99 |
| 9 | 2.79 | 2.57 | 3.90 | 4.23 |
| 10 | 2.50 | 2.07 | 1.12 | 1.72 |
| 11 | 3.22 | 3.03 | 2.47 | 2.13 |
| 12 | 1.27 | 1.09 | 1.27 | 5.66 |
| 13 | 6.60 | 7.90 | 7.35 | 7.00 |
| 14 | 2.94 | 1.76 | 2.53 | 3.05 |
| 15 | 1.65 | 3.24 | 2.46 | 2.36 |

**Table3.** MAE values using *coif*1 wavelet with different goal values and different training/validation images combinations.

| Goal | .0001 | .001 | .01 | .1 |
|---|---|---|---|---|
| Set# | | | | |
| 1 | 1.76 | 1.49 | 1.46 | 1.78 |
| 2 | 4.40 | 4.56 | 4.64 | 5.17 |
| 3 | 2.09 | 2.54 | 1.51 | 1.89 |
| 4 | 2.58 | 2.79 | 2.49 | 5.14 |
| 5 | 2.36 | 1.14 | 1.19 | 4.41 |
| 6 | 8.11 | 8.98 | 7.95 | 5.99 |
| 7 | 4.84 | 4.38 | 3.21 | 5.03 |
| 8 | 4.90 | 5.23 | 4.19 | 6.84 |
| 9 | 4.36 | 4.87 | 3.91 | 5.11 |
| 10 | 1.34 | 1.24 | 0.64 | 1.28 |
| 11 | 1.81 | 0.64 | 1.90 | 1.88 |
| 12 | 0.75 | 0.62 | 1.43 | 2.95 |
| 13 | 4.02 | 3.33 | 3.10 | 4.99 |
| 14 | 3.80 | 4.04 | 3.94 | 6.13 |
| 15 | 0.77 | 2.31 | 1.78 | 3.13 |

**Table4.** MAE values using *sym*3 wavelet with different goal values and different training/validation images combinations.

| Goal | .0001 | .001 | .01 | .1 |
|---|---|---|---|---|
| Set# | | | | |
| 1 | 1.71 | 2.66 | 2.03 | 2.10 |
| 2 | 3.04 | 4.09 | 3.85 | 5.03 |
| 3 | 2.19 | 3.57 | 2.73 | 2.72 |
| 4 | 3.77 | 5.18 | 3.88 | 5.72 |
| 5 | 3.72 | 2.06 | 2.83 | 2.13 |
| 6 | 7.85 | 8.25 | 8.30 | 8.31 |

| | | | | |
|---|---|---|---|---|
| 7 | 5.40 | 4.84 | 3.99 | 3.05 |
| 8 | 6.11 | 5.39 | 4.92 | 5.45 |
| 9 | 5.85 | 4.58 | 4.44 | 3.03 |
| 10 | 1.47 | 2.43 | 3.14 | 2.06 |
| 11 | 3.68 | 3.96 | 4.39 | 4.67 |
| 12 | 2.14 | 4.73 | 2.40 | 1.68 |
| 13 | 5.59 | 6.08 | 6.56 | 8.00 |
| 14 | 4.63 | 5.35 | 5.32 | 3.27 |
| 15 | 3.79 | 1.76 | 3.81 | 3.50 |

The minimum overall MAE=0.36 was achieved when Haar wavelet and a training goal value of 0.01 was used. This corresponds to a training combination using images of tilt angles 50° and 80° as validation images and the remaining images as training images. MAE values found using *db*4 are tabulated in Table 2. Again MAE for four different values of training goals are shown. The minimum MAE=1.09 corresponds to a goal value of 0.001 and a training combination using images of inclination angles of 40° and 80° as validation images and the remaining images as training images. Minimum MAE value found for *coif*1 is 0.62 at a goal of 0.001 and a training combination using images of inclination angles of 40° and 80° as validation images. For *sym*3 using tilt angles of 40° and 60° as validation angles with a goal of 0.0001 resulted in a minimum MAE of 1.47.

The minimum MAE obtained using Haar wavelet is smaller than the corresponding values for *db*4, *coif*1 and *sym*3 by several folds.

Tables 5 to 8 show MAE values found for the sets with best MAEs at different levels of SNR. In the Haar wavelet case, the best combination, at a goal value of 0.01, is very clearly superior to other goal values for all SNR values. However, such superiority is not noticed with other wavelets.

**Table5.** MAE for different goal values and minimum Haar overall MAE for different SNRs.

| Goal / SNR | 0.0001 | 0.001 | 0.01 | 0.1 |
|---|---|---|---|---|
| 3 | 0.62 | 3.38 | 0.23 | 2.21 |
| 6 | 1.00 | 3.78 | 0.34 | 2.38 |
| 9 | 1.17 | 3.69 | 0.53 | 2.50 |
| 12 | 1.09 | 4.44 | 0.33 | 3.12 |
| ∞ | 1.05 | 4.04 | 0.38 | 2.66 |
| average | 0.99 | 3.86 | 0.36 | 2.58 |

**Table6.** MAE for different goal values and minimum *db*4 overall MAE for different SNRs.

| Goal / SNR | 0.0001 | 0.001 | 0.01 | 0.1 |
|---|---|---|---|---|
| 3 | 1.88 | 0.73 | 0.55 | 5.66 |
| 6 | 2.47 | 2.22 | 2.10 | 6.33 |
| 9 | 0.38 | 0.90 | 1.32 | 5.21 |
| 12 | 1.20 | 0.92 | 1.70 | 6.19 |
| ∞ | 0.42 | 0.67 | 0.68 | 4.92 |
| average | 1.27 | 1.09 | 1.27 | 5.66 |

**Table7.** MAE for different goal values and minimum *coif*1 overall MAE for different SNRs.

| Goal / SNR | 0.0001 | 0.001 | 0.01 | 0.1 |
|---|---|---|---|---|
| 3 | 0.45 | 0.35 | 0.40 | 1.44 |
| 6 | 1.42 | 0.61 | 0.32 | 1.15 |
| 9 | 1.19 | 0.46 | 1.54 | 1.44 |
| 12 | 0.29 | 1.15 | 0.64 | 1.46 |
| ∞ | 0.40 | 0.51 | 0.33 | 0.92 |
| average | 0.75 | 0.62 | 0.64 | 1.28 |

**Table8.** MAE for different goal values and minimum *sym*3 overall MAE for different SNRs.

| Goal / SNR | 0.0001 | 0.001 | 0.01 | 0.1 |
|---|---|---|---|---|
| 3 | 2.15 | 1.16 | 1.31 | 0.79 |
| 6 | 1.75 | 2.06 | 2.77 | 1.41 |
| 9 | 1.45 | 1.57 | 2.45 | 2.64 |
| 12 | 1.04 | 2.62 | 1.85 | 2.36 |
| ∞ | 0.95 | 1.41 | 1.76 | 1.20 |
| average | 1.47 | 1.76 | 2.03 | 1.68 |

Based on the above findings, it is obvious that Haar wavelet with a goal value of 0.01 should be used in the present work for a minimum MAE value in determining tilt angles of PV modules.

Tables 9 to 12 show values obtained using the best training and validation pairs found for each wavelet. As can be seen, the systems estimations are very

close to the actual inclination angles for all wavelets and at all SNR values considered. However, the Haar wavelet's better performance is obvious again.

**Table9.** Predicted inclination angles in (°) for different SNRs using Haar wavelet minimum MAE settings.

| SNR | 3 | 6 | 9 | 12 | ∞ |
|---|---|---|---|---|---|
| Actual | | | | | |
| 50 | 50.28 | 49.54 | 48.98 | 49.36 | 49.35 |
| 80 | 79.82 | 80.21 | 79.95 | 80.01 | 80.12 |

**Table10.** Predicted inclination angles in (°) for different SNRs using *db*4 wavelet minimum MAE settings.

| SNR | 3 | 6 | 9 | 12 | ∞ |
|---|---|---|---|---|---|
| Actual | | | | | |
| 40 | 41.10 | 36.18 | 39.58 | 39.45 | 40.10 |
| 80 | 79.65 | 78.76 | 78.63 | 78.71 | 78.75 |

**Table11.** Predicted inclination angles in (°) for different SNRs using *coif*1 wavelet minimum MAE settings.

| SNR | 3 | 6 | 9 | 12 | ∞ |
|---|---|---|---|---|---|
| Actual | | | | | |
| 40 | 39.32 | 39.54 | 39.08 | 38.50 | 39.06 |
| 80 | 80.02 | 79.23 | 80.00 | 79.2 | 79.91 |

**Table12.** Predicted inclination angles in (°) for different SNRs using *sym*3 wavelet minimum MAE settings.

| SNR | 3 | 6 | 9 | 12 | ∞ |
|---|---|---|---|---|---|
| Actual | | | | | |
| 40 | 42.45 | 38.90 | 40.63 | 41.59 | 38.85 |
| 60 | 58.16 | 57.61 | 57.73 | 59.51 | 60.76 |

## *5. Conclusion*

A novel method to determine the inclination of PV tracking systems was introduced. The method utilizes optical images that can be acquired remotely to determine a PV module or array tilt angle. The image is preprocessed, followed by a 2D-DWT and an ANN processing. The results obtained using different ANN parameters and DWT families indicate the possibility of accurately detecting tilt angles. Haar wavelet seems to perform much better than the other wavelets considered in the work over a large range of SNR values.

## *6. References*


1. K.H. Solangi, M.R. Islam, R. Saidur, N.A. Rahim, H. Fayaz, A review on global solar energy policy, Renewable and Sustainable Energy Reviews 15 (2011) 2149–2163.

2. V.V. Tyagi, S.C. Kaushik, S.K. Tyagi, Advancement in solar photovoltaic/thermal (PV/T) hybrid collector technology, Renewable and Sustainable Energy Reviews, 16 (2012) 1383– 1398.

3. Halimeh Rashidi, Saeed Niazi and Jamshid Khorshidi, Adaptive Critic Based Neuro-Fuzzy Tracker for Improving Conversion Efficiency
in PV Solar Cells, Research Journal of Applied Sciences, Engineering and Technology 15, 4 (2012) 2316-2322.

4. M. Koussa, A. Cheknane, S. Hadji, M. Haddadi and S. Noureddine, Measured and modelled improvement in solar energy yield from flat plate photovoltaic systems utilizing different tracking systems and under a range of environmental conditions
, Applied Energy, 88, 5 (2011) 1756-1771.

5. Taher Maatallah, Souheil El Alimi, Sassi Ben Nassrallah, Performance modeling and investigation of fixed, single and dual-axis tracking, photovoltaic panel in Monastir city, Tunisia, Renewable and Sustainable Energy Reviews 15 (2011) 4053–4066.

6. Alasdair Miller and Ben Lumby, Utility Scale Solar Power Plants, A Guide For Developers and Investors, IFC, World bank Group, Feb2012.

7. B. Yegnanarayana, Artificial Neural Networks, PHI Learning Pvt. Ltd., Aug 1, 2004, pp19.

8. Markos Markou, Sameer Singh, Noveltydetection: a review—part 2:neural network based approaches, Signal Processing 83 (2003) 2499 – 2521.

9. A. Al-Lawati and H. Bourdoucen, Improvement of RMSE in optical fiber communication systems using RBF ANN post processing approach, The Journal of Electrical Engineering, 11, 1 (2011) 9-12.

10. Hamid Khorrami, Majid Moavenian, A comparative study of DWT, CWT and DCT transformations in ECG arrhythmias classification. Expert Systems with Applications 37 (2010) 5751–5757.

11. Ali N. Akansu, Wouter A. Serdijn, Ivan W. Selesnick, Emerging applications of wavelets: A review, Physical Communication 3 (2010) 1_18.

12. Christopher E. Heilt, David F. Walnut, Continues and discrete wavelet transforms., Society for Industrial and Applied Mathematics, 31, 4 (1998) 826-666.

13. Antonini, M., Valbonne ,Barlaud, M. ; Mathieu, P. ; Daubechies, I. Image compression using the 2-D

wavelet transform, IEEE Transactions on Image Processing, 1, 2 (1992) 205 – 220.

14. Chun-Lin, Liu, A Tutorial of the Wavelet Transform, http://disp.ee.ntu.edu.tw/tutorial/WaveletTutorial.pdf, February 23, 2010.